Published in final edited form as:

Pediatr Res. 2013 March ; 73(3): 277–285. doi:10.1038/pr.2012.180.

Ovine uterine space restriction alters placental transferrin receptor and fetal iron status during late pregnancy

Mary Y. Sun[1,2], **Jason M. Habeck**, **Katie M. Meyer**[1,2,3], **Jill M. Koch**[2], **Jayanth Ramadoss**[2], **Sharon E. Blohowiak**[1], **Ronald R. Magness**[1,2,3], and **Pamela J. Kling**[1]

[1]Department of Pediatrics, Perinatal Research Laboratory, University of Wisconsin, Madison, WI

[2]Department of Obstetrics and Gynecology, Perinatal Research Laboratory, University of Wisconsin, Madison, WI

[3]Department of Animal Sciences, Perinatal Research Laboratory, University of Wisconsin, Madison, WI

Abstract

Background—Fetal growth restriction is reported to be associated with impaired placental iron transport. Transferrin receptor (TfR) is a major placental iron transporter in humans, but is unstudied in sheep. TfR is regulated by both iron and nitric oxide (NO), the molecule produced by endothelial NOS (eNOS). We hypothesized that limited placental development downregulates both placental TfR and eNOS expression, thereby lowering fetal tissue iron.

Methods—An ovine surgical uterine space restriction (USR) model, combined with multifetal gestation, tested the extremes of uterine and placental adaptation. Blood, tissues, and placentomes from non-space restricted (NSR) singletons were compared to USR fetuses at 120 or 130 days of gestation (GD).

Results—When expressed proportionate to fetal weight, liver iron content did not differ while renal iron was higher in USR vs. NSR fetuses. Renal TfR protein expression did not differ, but placental TfR expression was lower in USR fetuses at GD130. Placental levels of TfR correlated to eNOS. TfR was localized throughout the placentome, including the hemophagous zone, implicating a role for TfR in ovine placental iron transport.

Conclusion—In conclusion, fetal iron was regulated in an organ-specific fashion. In USR fetuses, NO-mediated placental adaptations may prevent the normal upregulation of placental TfR at GD130.

INTRODUCTION

Uterine anomalies and multifetal gestations are two independent, and increasingly common, clinical factors associated with IUGR (1, 2), IUGR ultimately increases the risk of adult-

Corresponding Author: Pamela J. Kling, MD Department of Pediatrics University of Wisconsin and Meriter Hospital 202 S. Park St. Madison, WI 53715 pkling@pediatrics.wisc.edu 608-417-5867 Phone 608-417-6377 Fax.

Conflict of interest: None

onset diseases, including impaired renal development and hypertension, as described by the Barker hypothesis of developmental origins of adult disease (3). Current practices in assisted reproductive technologies increase both conception rates and multifetal pregnancies in women with uterine anomalies (4). In human twins, hypertension and impaired renal development are reported in the smaller twin (5), but the impact of multifetal gestation or reduced space for placental development on fetal kidney development remains unknown. Sheep can be used to model multifetal gestation and the impact of reduced space on placental function, fetal growth, and renal development (6, 7), an advantage because nephrogenesis ends at 80% of gestation in both humans and sheep (8).

An important pathological etiology in IUGR is depletion of fetal tissue iron (9). Impaired fetal iron delivery is linked to both renal structural anomalies and hypertension (10, 11). However, virtually nothing is known about placental iron transfer in multifetal gestation and/or reduced uterine space. In mammals, iron transport to the fetus is accomplished by three recognized pathways: 1) iron-rich endometrial gland secretions; 2) endocytosis of transferrin (Tf)-bound iron through transferrin receptors (TfR); and 3) trophoblast ingestion of pooled maternal erythrocytes in the hemophagous zone (12-14). Although detailed mechanisms are not described in sheep, the ovine model confers the advantage of utilizing all three pathways for fetal iron acquisition (12).

Transferrin receptor (TfR) is the major iron transporter in most tissues, including human and rodent placentae (15, 16), but its role in sheep has not been described. TfR expression is regulated by cellular iron levels (16). Placental TfR was increased after mild gestational iron deficiency anemia (IDA) in humans (15) and in IDA-induced IUGR in rats, with expression inversely related to fetal liver iron levels (16). In contrast, placental TfR expression was lower in singleton human IUGR (17), perhaps from poor uteroplacental blood flow (9). In addition to iron, nitric oxide (NO), produced by the enzyme endothelial NOS (eNOS), can regulate TfR expression (18). Because NO is vital to placental function (19), examining the interplay between placental TfR and nitric oxide (NO) in the context of multifetal gestation and/or limited uterine space should provide a better understanding of iron transport mechanisms.

We previously reported an ovine uterine space restriction (USR) model (7) with reduced space for placentomal development combined with multifetal gestation that caused asymmetrical IUGR. The role of eNOS and NO in regulating placental TfR expression, fetal iron status, and fetal kidney development in multifetal gestation can be investigated using this model. We hypothesize that placental iron transporter expression in USR will be downregulated by eNOS and be reflected by lower fetal liver and kidney iron contents. Our aims were to: 1) evaluate the impact of limited space for placental development on maternal iron status, placental TfR expression, and fetal liver iron status; 2) investigate the interplay between iron status and impaired renal development; and 3) evaluate the association between TfR and eNOS expression in both the placenta and kidney.

RESULTS

Fetal and Placental Morphometry

This fetal cohort consisted of 12 non-space restricted (NSR) and 12 USR fetuses at gestational day (GD) 120, and 10 NSR and 19 USR fetuses at GD130 (Table 1). As we previously published (7), this cohort exhibited placental adaptation and lower placental efficiency, greater fetal weight-to-placental weight, and asymmetric IUGR with brain sparing in USR between GD120 and GD130. Growth arrest in USR at GD130 was seen, as measured by fetal body, kidney, and liver weights (Table 1). Fetal weight (kg) in USR fetuses did not differ from NSR at GD120, but a growth arrest was seen over time, resulting in 40% lower weight in USR versus NSR at GD130 ($p<0.005$). In USR, fetal kidney weight (g) was unchanged between GD120 and GD130, but was 19% lower ($p<0.005$) and 29% lower ($p<0.001$) than NSR at GD120 and GD130, respectively. Mean kidney weight expressed proportionate to fetal weight (g/kg) in USR did not differ from NSR at either time point, but the ratio (g/kg) fell 20% between GD120 and GD130 in both USR and NSR, ($p<0.005$). In USR fetuses, liver weight (g) was unchanged over time, but was 17% lighter ($p<0.05$) and 33% lighter ($p<0.0001$) compared to NSR at GD120 and GD130, respectively. Liver weight adjusted to fetal weight (g/kg) between USR and NSR fetuses did not differ at either time point, but the ratio in either group was 26% lower at GD130, compared to GD120, ($p<0.0001$) (Table 1).

Compared to NSR, total placentome weight (g) was 56% heavier in the USR group ($p<0.0001$) at GD120, and 48% heavier ($p<0.0001$) in the USR group at GD130 (Table 1). Placentome weight per individual fetus, i.e. proportionate to fetal number, was 25% lower ($p<0.001$) in the USR group at GD120 and 39% lower ($p<0.001$) at GD130 compared to NSR (Table 1).

Maternal and Fetal Circulating Iron Indices

Because 75% of body iron is present in erythrocytes, maternal and fetal RBC count, hematocrit, and mean cell volume (MCV) were examined (Table 2). There were no differences seen at GD120 between groups for all erythrocyte iron indices. At GD130, maternal RBC count was 15% lower ($p<0.05$) in USR than NSR, but maternal MCV, plasma iron and total iron binding capacity (TIBC) did not differ, while transferrin (Tf) saturation was 26% higher ($p<0.05$). We found no relationship between maternal total mg of circulating iron and total mg of circulating iron in the combined fetoplacental unit (R=-0.175 $P=0.3$). Fetal RBC counts and calculated total mg of circulating iron per fetus did not differ between USR and NSR groups at GD130. In USR at GD130 fetal MCV was 6% lower and fetal Tf saturation was 30% lower than NSR ($p<0.05$). However, because fetal TIBC was 40% higher ($p<0.05$), plasma iron was unchanged, compared to NSR (Table 2).

Fetal Liver Iron Assessment

Fetal liver iron concentration (μg/g wet weight) of NSR vs. USR was not different at either GD120 or GD130 (Table 3). At GD120, similar total fetal liver non-heme iron allotment (μg) was seen, but at GD130, USR was 36% lower than NSR at GD130 ($p<0.05$). Liver iron

expressed proportionate to fetal weight (μg/kg) was similar in both groups and times (Table 3).

Fetal Kidney Iron Assessment

Fetal kidney non-heme iron concentration (μg/g wet weight) was not different between treatments at GD120, but was greater in USR at GD130 compared to NSR (Table 4). Surprisingly, fetal kidney iron allotment (μg) in the USR was higher than NSR at GD120, but it was similar in both groups at GD130. However, kidney iron was 27% and 37% greater when adjusted proportionate to fetal weight (μg/kg) in USR than NSR at both time points ($p<0.05$), respectively (Table 4).

Fetal Kidney TfR and eNOS Expression

Immunohistochemistry for all groups and time points showed TfR expression in the glomeruli, maculae densa, and distal and proximal tubules (Figure 1a). Tubular epithelial TfR staining was seen on both the luminal surface and within endocytic vesicles. Initial assessment of TfR expression in kidney found virtually no differences in tissue localization or intensity between treatments or between GD groups, so immunoblot was performed instead of quantitative morphometric analysis. Enhanced Prussian Blue (PB) staining showed intracellular iron deposits in phagocytic cells and within the glomeruli and tubular epithelium in kidneys of some USR fetuses (Figure 1b), but none were observed in NSR. In fetal kidney tissue, normalized TfR protein by immunoblot showed no difference between groups at either gestation (Figure 2). To determine the relationship between NO and TfR expression, renal eNOS expression by immunoblot was determined. We observed no difference in renal eNOS expression in both groups at both time points ($p>0.05$) (Figure 2). Kidney TfR expression was not related to kidney eNOS expression ($r=0.02$, $p=0.95$).

Placentome TfR and eNOS Expression

For all groups at all time points, TfR staining was found in uterine glands, and maternal and fetal components of the placentome (Figure 1c-d). Prominent TfR staining was also localized to the chorionic epithelium of the hemophagous region with apical microvilli encircling maternal erythrocytes via endocytic vesicles for both groups and time points (Figure 1e). Rust colored staining of partially degraded erythrocyte hemoglobin (see circles) was seen but additional staining for TfR also surrounded the encircled erythrocytes (Figure 1e). Initial assessment of placentomal TfR expression found virtually no differences in tissue localization or intensity between treatments or between GD groups, so immunoblot was performed instead of quantitative morphometric analysis. Immunoblot analyses revealed that placental TfR expression was not different between NSR and USR groups at GD120 (Figure 3). However, at GD130, TfR expression was 40% lower in USR, compared to NSR ($p<0.0001$). In contrast to TfR, compared to GD120 levels, placental eNOS expression was 4-fold higher in NSR ($p<0.005$) and 6-fold higher in USR ($p<0.05$) by GD130 (Figure 3).

Using all samples regardless of GD and uterine space condition, placental TfR expression was positively correlated with placental eNOS expression ($r=0.726$; $p<0.001$) (Figure 4). Placental TfR and fetal liver non-heme iron did not correlate ($r=0.06$, $p=0.8$).

DISCUSSION

This study is the first in-depth examination of the effects of maternal and fetal iron metabolism in IUGR sheep. We utilized our previously described model of IUGR induced by multifetal gestation and restricted surface area for placental development (7) to investigate whether IUGR caused from USR exhibited iron metabolism similar to placental insufficiency-induced IUGR or gestational IDA-induced IUGR. Our findings are important because of the space limitations seen in 5.5% of human pregnancies with uterine structural anomalies (20) and the 3% of human pregnancies carrying multiple fetuses (1). Similar to both placental insufficiency and gestational IDA, we observed asymmetric IUGR in USR, with proportionately smaller liver and kidney weights. In USR we found normal maternal iron status and observed neither decreased nor increased fetal RBC mass. In USR, fetal liver iron (μg) was proportionately lower, but kidney iron (μg) was similar, but higher proportionate to fetal weight compared to NSR, inconsistent with IUGR from either gestational IDA or placental insufficiency. We are the first to show that ovine placenta employs TfR. Unlike gestational IDA, placental TfR expression was correlated with placental eNOS expression, but not liver iron.

The risk for maternal iron deficiency anemia (IDA) increases 4-fold during singleton human pregnancies (21). IDA during pregnancy can contribute to IUGR (21) and carrying multiple fetuses further increases maternal risk for IDA because of greater fetal iron needs (22). Blood hematological indices were unlike either gestational IDA- or placental insufficiency-induced IUGR. Although the USR ewes exhibited lower hemoglobin, higher maternal Tf saturation supported normal ewe iron status. The fetuses were not anemic, but were mildly microcytic (smaller MCV). Fetal MCV is a suboptimal index of ID because immature RBCs are larger (higher MCV) than mature RBC (23). Although fetuses exhibit a greater proportion of immature RBCs, it is likely that smaller fetal MCV represents relatively fewer immature fetal RBCs produced resulting from the growth arrest. Although we found greater fetal TIBC (via higher Tf levels), circulating plasma iron was higher in USR at GD 130, inconsistent with fetal iron depletion. Based on the calculated total iron needs of the combined fetoplacental units, we found no association between maternal supply and fetal demand. These data support that the USR ewe adapted to the greater fetal iron body mass (and iron needs) by increasing ewe plasma Tf saturation. The fetuses adapted to USR by increasing plasma transport iron capacity. These findings are distinct from human or animal gestational IDA-induced IUGR (16, 24). Additionally, unlike placental insufficiency-induced IUGR, the USR group had normal ewe hematocrit, ewe iron status (25), and fetal liver iron concentration (26).

Fetal renal iron depletion is reported to accompany IUGR and impair renal development (10). The current study is the first to directly measure fetal renal iron levels after any etiologic cause of IUGR. We observed that liver iron was proportionate to fetal weight, but kidney iron was conserved and regulated based on amount needed to support normal growth. In contrast to our hypothesis of depleted kidney iron in USR-induced IUGR, the reverse was seen. The apparent difference in how kidney iron is regulated versus liver could be due to the umbilical vein anatomy delivering iron directly to the liver before other fetal organs. The liver is critical for iron storage and is exquisitely sensitive to iron overload, necessitating

tight iron regulatory mechanisms via hepcidin (27). Liver hepcidin serves as the master regulator of iron homeostasis, controlling liver iron uptake or release from hepatocytes via plasma Tf. In gestational IDA, hepcidin plays a major role in controlling fetal liver iron (16). However, unlike liver, hepcidin does not control kidney iron trafficking (28), providing a potential explanation for the differences in organ iron regulation.

Fetal renal tubular cells possess luminal TfR and import Tf-bound iron from the filtered urine, instead of via plasma Tf, which possibly explains why there was no observed association between renal eNOS and TfR (28). Renal iron content (μg) could be determined by the relatively constant fetal glomerular filtration. We also observed TfR staining of tubules, including the specialized distal tubules called the maculae densa, key regulators of renin release from the juxtaglomerular cells. The renin-angiotensin system plays a key role in nephrogenesis (29), as well as its role in regulating salt balance and blood pressure. The interplay between renin-angiotensin signaling and renal iron concentration has been described (29), but not previously in fetuses. Thus, the greater renal iron could be an adaptive protective mechanism for current survival needs, especially in light of needs for ongoing nephrogenesis and tubular elongation. However, consistent with the developmental origins of adult disease, this response could also be maladaptive in the long term by altering the expression of key renal genes (3). Based on higher renal iron content, TfR expression should have been downregulated, but it was not. Further, iron 2+/3+ deposits on enhanced PB staining are not normally seen in kidneys, but were seen in tubules, glomeruli, and phagocytic cells in some USR fetuses. The combination of high iron concentrations and iron deposits suggest that iron excess, instead of deficiency, may disrupt nephrogenesis due to the catalytic potential of unbound iron, which warrants further investigation.

Fetal liver was examined because it regulates plasma iron and Tf levels, storage iron, and also controls placental iron transport, based on fetal iron needs (16, 26). In both USR and NSR groups, fetal liver iron appears to be regulated proportionate to fetal weight. In contrast to the lower blood and tissue iron seen in term human fetuses with placental insufficiency-induced IUGR (26), the current study observed normal fetal blood iron content, but greater iron binding capacity effectively delivering a proportionate amount of iron to the fetal liver. The difference between our findings and other models of IUGR could be timing, as we studied fetuses at 80-90% of term gestation and not term. The current data also directly contrast to findings of lower fetal liver iron correlating to placental TfR in the rat gestational IDA model (16). These conflicting results may be due to supply/demand relationships, with our study demonstrating greater ewe iron supply permitting placental adaptation (7). However, the current study is partly consistent with rat studies that found no relationship between placental TfR and fetal liver iron until liver iron fell below a critical level (16).

TfR, the major iron transporter in the mammalian placenta (16), was 40% lower in USR than NSR at GD130. This finding was less striking than three-fold lower TfR protein expression in IUGR placentae of human placental-insufficiency singletons (17) or the three-fold higher placental TfR mRNA expression in rats with gestational IDA (16). There appears to be no developmental difference in pattern of distribution of TfR between GD 120 and GD 130, perhaps because the hemophagous zone is fully developed and both time points are temporally located during the rapid growth trajectory that drives iron transfer. A greater

difference in distribution might be seen with sampling in early second trimester or term (GD147).

TfR levels are regulated by both intracellular iron and NO (30, 31). NO is a rapidly-acting molecule catalyzed by NOS with high affinity for iron containing metalloproteins (31). Ovine placental endothelial NOS (eNOS) levels normally rise during gestation, promoting uterine artery dilation via NO (19). Placental eNOS correlates to NO levels, with lower expression in sheep or human IUGR (32). *In vivo* and *in vitro* work (18) show NO may increase levels from greater TfR mRNA stability (33). Stable placental TfR expression is seen in normal human pregnancy (24), lower expression in placental insufficiency (17), and higher expression in gestational IDA-induced IUGR (16).

The relationship between NO and TfR in placenta was studied. Consistent with previous work (19), placental eNOS levels increased as gestation progressed in both USR and NSR, but trended lower in USR than NSR at both time points. However, kidney eNOS expression is reported to be constant throughout gestation and between treatments (34). NO, produced by renal NOS enzymes, is a major vasodilatory factor in renal, and systemic circulations, controlling renal blood pressure (35). We observed no relationship between TfR and eNOS expression in the kidney, but found a direct relationship between placental TfR and eNOS, supporting that eNOS plays a role in placental adaptations enabling maternal-to-fetal iron transfer. In keeping with this assertion, we previously observed a dramatic rise in uterine blood flow and eNOS in the gravid versus nongravid horn in pregnancies after unilateral ligation (36). Greater eNOS and NO production improve uterine blood flow (37). Our findings support a possible link between NO, blood flow, and maternal-to-fetal iron transport.

The interaction between NO and TfR had not previously been studied in the placenta; thus our findings of a direct relationship between placental TfR and eNOS is novel and important. Although iron regulates TfR expression via cytosolic iron regulatory proteins (IRPs), NO also regulates TfR (31). IRPs bind to hairpin structures called iron response elements (IREs) on untranslated regions of TfR mRNA, based on intracellular levels of either iron or NO (33). NO increases binding of IRP1, improving iron transport (TfR synthesis) and repressing iron storage (33), but the reverse may occur under oxidizing conditions (30). The direct relationship between eNOS and TfR support a role for NO in upregulating placental TfR synthesis (18).

The ovine model confers the advantage of utilizing all three mechanisms for fetal iron acquisition; through iron-rich endometrial gland secretions, endocytosis of Tf-bound iron from maternal circulation through TfR, and ingestion of maternal erythrocytes (12, 13). We report for the first time TfR expression in uterine glands, uniform TfR localization on both the maternal villus and the fetal chorionic epithelium, and most importantly, the presence of TfR in the hemophagous zone. Hemophagous zones are the sites where maternal erythrocytes pool and internalize via endocytosis into the chorionic epithelium via microvilli, where erythrocytic hemoglobin is degraded (12), and iron is reported to be transferred to the fetus. However, the complete mechanism for iron transport in hemophagous zones is incompletely elucidated. TfR was localized throughout the epithelia

of the hemophagous zone, supportive of a role in iron transport because cell surface TfR located on microvilli normally undergo endocytosis. Focusing our investigation on the hemophagous zone enables examination of the important final steps of iron trafficking out of trophobasts into neighboring interstitium and fetal endothelium. Interestingly, we found virtually no Fe2+ or Fe3+/hemosiderin by enhanced PB staining near the hemophagous zone (*data not shown)*. Trophoblasts are reported to be minor depots of hemosiderin iron (38), and iron not stored is exported, through one of the iron exporters (15), taken up by interstitial Tf, and finally, imported to fetal endothelium via TfR (16). We are the first to show localization of TfR in both fetal villous and endothelial cells adjacent to the hemophagous zones in ovine placentomes, supporting the role of TfR in transporting iron through the hemophagous zone into fetal circulation.

In summary, this ovine USR IUGR model differs from both placental insufficiency-induced IUGR and gestational IDA-induced IUGR, because we observed fetal liver iron concentration proportionate to body weight. USR fetuses also exhibited proportionately higher kidney iron relative to body weight, but it is unclear whether this adaption is advantageous or contributes to long-term maladaptation in kidney function. Although fetal kidney iron was regulated differently than fetal liver, we hypothesize that placental TfR expression in USR fetuses did not rise to the same degree as in the NSR group to avoid oversaturating the fetal liver, an organ exquisitely susceptible to iron toxicity. TfR plays a role in all three recognized pathways for fetal iron acquisition; in iron-rich endometrial glands, in the maternal-fetal interface, and in the hemophagous zone. The strong relationship between placental levels of eNOS and TfR demonstrates a potential role for NO in mediating placental-to-fetal iron transport to maintain fetal iron content during a compromised uterine placental development. A better understanding of placental and fetal iron trafficking is necessary to elucidate the mechanisms in alterations of fetal development in all etiologies of IUGR.

METHODS

Animals

Animal protocols were approved by University of Wisconsin–Madison Research Animal Care and Use Committee. Ewes of mixed Western breeds (n=32) were group housed and fed a mixture of hay and corn silage that met daily feed requirements of pregnant sheep. Surgical and synchronization procedures were described by Meyer et al. (7). Ewes were randomly assigned to one of two treatment groups; unilateral uterine horn ligation to limit uterine space for placental development or nonunilateral ligation (Table 5). Unilateral ewes underwent complete disconnection of a single uterine horn and intercornual vascular connections at least 2 months before breeding to a fertile ram. A synchronization protocol was performed using an intravaginal controlled internal drug release (Progesterone CIDR; 0.3 g; Pfizer, Aukland, New Zealand) for 10-14 days, followed by intramuscular prostaglandin $F_2\alpha$ (15 mg; Pfizer) and equine chorionic gonadotropin (500 IU; EMD Biosciences, San Diego, CA) injections (7). Pregnancy was confirmed by ultrasound by GD60.

Fetal Measurements and Tissue Collection

We utilized a smaller cohort of fetuses than previously reported (7), with twins excluded to further demarcate USR fetuses from NSR. Nonsurvival surgery using sodium pentobarbital (50 mg·mL^{-1}) was performed on either GD120 (120.4; n=16 ewes) or GD130 (129.9; n=16 ewes) term 147 days. Approximately 12 mL of heparinized blood from the maternal jugular vein, and simultaneously fetal umbilical vein and artery were collected prior to fetal removal and euthanasia. Placentomes, fetal liver, and fetal kidneys were weighed, and frozen at −80°C. Fresh whole blood was analyzed for indices of erythrocyte iron (RBC, hemoglobin, MCV) using pocH-100i laboratory analyzer (Sysmex, Mundelein, IL). Blood was centrifuged for 10 minutes at 3600 x g at 4°C and plasma stored at −80°C for plasma transferrin Tf and Tf saturation. Total circulating iron was calculated as (weight × hemoglobin × 3.42 × 1.25)/1000. TIBC was measured by the FerroZine method using an Unbound Iron Binding Capacity assay kit (Thermo Scientific, Middletown, VA). Plasma Tf concentration (mg/dL) was calculated as TIBC/2 (39).

Utilizing placentome number and total placentome weight per fetus, fetuses were grouped as NSR: nonunilateral singleton fetuses (n=9) and unilateral singletons (n=13), or USR: nonunilateral triplets (n=21), nonunilateral quadruplets (n=4), and unilateral triplets (n=6) (7), with treatment and gestation groupings shown in Table 5. NSR was defined as one fetus per horn, while USR was defined as more than one fetus per horn.

Liver and Kidney Non-Heme Iron Assay

Fetal liver and kidneys were homogenized in iron free water with an iron free pestle homogenizer. Kidney and liver non-heme iron concentration (μg/g wet weight), total non-heme iron allotment (μg), and total non-heme iron content proportional to fetal weight (μg/kg) were quantified (40).

Kidney and Placentome Histology and Immunohistochemistry (IHC)

Formalin fixed paraffin embedded fetal kidneys underwent histological and immunohistochemical analysis on 10 μm sections. Enhanced PB staining was performed to identify iron 2+ and 3+ deposits (41). Immunohistochemistry was used to examine TfR distribution (19). Slides were deparaffinized with HistoClear (National Diagnostics, Atlanta, GA) and rehydrated in graded ethanol. Peroxidase activity was blocked with 3% hydrogen peroxide. Antigen retrieval step was performed by boiling tissue in a 0.1 M citrate buffer (42). Primary rabbit polyclonal anti-human TfR1 antibody (1:50; Santa Cruz Biotechnology, Santa Cruz, CA), rabbit monoclonal anti-TfR antibody (1:50; Santa Cruz Biotechnology), and biotinylated anti-rabbit IgG secondary antibody from Vector Labs' Universal ABC Kit (Vector Labs, Burlingame, CA), stained with DAB (Vector Labs) and counterstained with Hematoxylin (Fisher Scientific, Pittsburgh, PA).

Kidney and Placentome Western Blot

Either frozen placentome or fetal kidney was homogenized in MAPK lysis buffer and centrifuged at 16,000 x g for 15 minutes at 4°C. Immunoblot analysis was performed as previously described(43). Monoclonal anti-TfR1 CD71 (1:5000; Santa Cruz Biotechnology), monoclonal eNOS (1:3000 BD Laboratories, Franklin Lakes, NJ), monoclonal β-actin

(1:3000 Cell Signaling, Danvers, MA), and monoclonal GAPDH (1:3000 BD Laboratories) were used. Membranes were visualized with an ECL detection kit (Fisher Scientific). Films were developed and quantified using densitometry.

Data Analysis

Statistical analyses were performed using a two-way ANOVA followed by a Student-Newman-Keuls *post hoc* test and simple linear regression using SigmaStat 1.0 software (Jandel Corporation, San Rafael, CA). Immunoblot optical densities were normalized to either β-actin (placenta) or GAPDH (kidney) expression and further standardized as fold difference of NSR at GD120. Data are presented as Means ± SEM, with $p<0.05$ considered significant.

Supplementary Material

Refer to Web version on PubMed Central for supplementary material.

ACKNOWLEDGMENTS

Manuscript assistance was provided by Sheikh Omar Jobe, Timothy J. Morschauser, and Mayra B. Pastore. Technical support was provided by Jason L. Austin, Kreg M. Grindle, Gladys E. Lopez, Terrance M. Phernetton, and Patrick J. Halbach, as well as Todd A. Taylor at the University of Wisconsin Arlington Farm Facility. This manuscript has minimal overlap with previously published data in the published article by Meyer et al (7). This work is in partial fulfillment of the PhD degree of the Interdepartmental Graduate Program in Nutritional Sciences.

Statement of financial support: National Institutes of Health grants HL49210, HD38843, HL087144 (to RRM), and HL087144 Supplement (to PJK); Meriter Foundation (to PJK); and University of Wisconsin Department of Pediatrics (to PJK).

REFERENCES

1. Martin JA, Hamilton BE, Sutton PD, Ventura SJ, Mathews TJ, Osterman MJ. Births: final data for 2008. Natl Vital Stat Rep. 2010; 59(1):1, 3–71.
2. Resnik R. Intrauterine growth restriction. Obstet Gynecol. 2002; 99(3):490–6. [PubMed: 11864679]
3. Barker DJ, Eriksson JG, Forsen T, Osmond C. Fetal origins of adult disease: strength of effects and biological basis. Int J Epidemiol. 2002; 31(6):1235–9. [PubMed: 12540728]
4. Monteagudo A, Strok I, Greenidge S, Timor-Tritsch IE. Quadruplet pregnancy: two sets of twins, each occupying a horn of a septate (complete) uterus. J Ultrasound Med. 2004; 23(8):1107–11. quiz 12-3. [PubMed: 15284471]
5. Bergvall N, Iliadou A, Johansson S, et al. Genetic and shared environmental factors do not confound the association between birth weight and hypertension: a study among Swedish twins. Circulation. 2007; 115(23):2931–8. [PubMed: 17515462]
6. Gootwine E, Spencer TE, Bazer FW. LItter-size-dependent interauterine growth restriction in sheep. Animal. 2007; 1:547–64. [PubMed: 22444412]
7. Meyer KM, Koch JM, Ramodoss J, Kling PJ, Magness RR. Ovine surgical model of uterine space restriction: Interactive effects of uterine anomalies and multi-fetal gestations on fetal and placental growth. Biol Reprod. 2010; 83:799–806. [PubMed: 20574052]
8. Wintour EM, Moritz KM, Johnson K, Ricardo S, Samuel CS, Dodic M. Reduced nephron number in adult sheep, hypertensive as a result of prenatal glucocorticoid treatment. J Physiol. 2003; 549:3–929. [PubMed: 12651923]
9. Georgieff MK, Mills MM, Gordon K, Wobken JD. Reduced neonatal liver iron concentrations after uteroplacental insufficiency. J Pediatr. 1995; 127(2):308–4. [PubMed: 7636662]

10. Lisle SJM, Lewis RM, Petry CJ, Ozanne SE, Hales CN, Forhead AJ. Effect of maternal iron restriction during pregnancy on renal morphology in the adult rat offspring. Brit J Nutr. 2003; 90:33–9. [PubMed: 12844373]
11. Gambling L, Dunford S, Wallace DI, et al. Iron deficiency during pregnancy affects postnatal blood pressure in the rat. J Physiol. 2003; 552(2):603–10. [PubMed: 14561840]
12. Burton GJ, Samuel CA, Steven DH. Ultrastructural studies of the placenta of the ewe: phagocytosis of erythrocytes by the chorionic epithelium at the central depression of the cotyledon. Q J Exp Physiol Cogn Med Sci. 1976; 61(4):275–86. [PubMed: 1050016]
13. Myagkaya GL, Schornagel K, van Veen H, Everts V. Electron microscopic study of the localization of ferric iron in chorionic epithelium of the sheep placenta. Placenta. 1984; 5(6):551–8. [PubMed: 6527986]
14. Pereira FT, Braga FC, Burioli KC, et al. Transplacental transfer of iron in the water buffalo (Bubalus bubalis): uteroferrin and erythrophagocytosis. Reproduct Domest Anim. 2010; 45(5): 907–14.
15. Li YQ, Yan H, Bai B. Change in iron transporter expression in human term placenta with different maternal iron status. Eur J Obstet Gynecol Reprod Biol. 2008; 140(1):48–54. [PubMed: 18586377]
16. Gambling L, Czopek A, Andersen HS, et al. Fetal iron status regulates maternal iron metabolism during pregnancy in the rat. Am J Physiol Regul Integr Comp Physiol. 2009; 296(4):R1063–70. [PubMed: 19176888]
17. Mando C, Tabano S, Colapietro P, et al. Transferrin receptor gene and protein expression and localization in human IUGR and normal term placentas. Placenta. 2011; 32(1):44–50. [PubMed: 21036394]
18. Wang H, Duan X, Liu J, Zhao H, Liu Y, Chang Y. Nitric Oxide contributes to the regulation of iron metabolism in skeletal muscle in vivo and in vitro. Mol Cell Biochem. 2010; 342(1-2):87–94. [PubMed: 20411304]
19. Zheng J, Li Y, Weiss AR, Bird IM, Magness RR. Expression of endothelial and inducible nitric oxide synthases and nitric oxide production in ovine placental and uterine tissues during late pregnancy. Placenta. 2000; 21(5-6):516–24. [PubMed: 10940202]
20. Chan YY, Jayaprakasan K, Zamora J, Thornton JG, Raine-Fenning N, Coomarasamy A. The prevalence of congenital uterine anomalies in unselected and high-risk populations: a systematic review. Hum Reprod Update. 2011; 17(6):761–71. [PubMed: 21705770]
21. Scholl TO. Iron status during pregnancy: setting the stage for mother and infant. Am J Clin Nutr. 2005; 81:1218S–22S. [PubMed: 15883455]
22. Bdolah Y, Lam C, Rajakumar A, et al. Twin pregnancy and the risk of preeclampsia: bigger placenta or relative ischemia? Am J Obstet Gynecol. 2008; 198(4):428, e1–6. [PubMed: 18191808]
23. Blohowiak SE, Chen ME, Repyak KS, et al. Reticulocyte enrichment of zinc protoporphyrin/heme discriminates impaired iron supply during early development. Pediatr Res. 2008; 64:63–7. [PubMed: 18360311]
24. Bradley J, Leibold EA, Harris ZL, et al. Influence of gestational age and fetal iron status on IRP activity and iron transporter protein expression in third-trimester human placenta. Am J Physiol. 2004; 287(4):R894–901.
25. Soubasi V, Petridou S, Sarafidis K, et al. Association of increased maternal ferritin levels with gestational diabetes and intra-uterine growth retardation. Diabetes Metab. 2010; 36(1):58–63. [PubMed: 20074991]
26. Chockalingam UM, Murphy E, Ophoven JC, Weisdorf SA, Georgieff MK. Cord transferrin and ferritin values in newborn infants at risk for prenatal uteroplacental insufficiency and chronic hypoxia. J Pediatr. 1987; 111:283–6. [PubMed: 3612404]
27. Pietrangelo A. Hemochromatosis: an endocrine liver disease. Hepatology. 2007; 46(4):1291–301. [PubMed: 17886335]
28. Smith CP, Thevenod F. Iron transport and the kidney. Biochim Biophys Acta. 2009; 1790(7):724–30. [PubMed: 19041692]

29. Ishizaka N, Saito K, Furuta K, et al. Angiotensin II-induced regulation of the expression and localization of iron metabolism-related genes in the rat kidney. Hypertens Res. 2007; 30:195–202. [PubMed: 17460390]
30. Kim S, Ponka P. Nitric oxide-mediated modulation of iron regulatory proteins: implication for cellular iron homeostasis. Blood Cells Mol Dis. 2002; 29(3):400–10. [PubMed: 12547230]
31. Mladenka P, Simunek T, Hubl M, Hrdina R. The role of reactive oxygen and nitrogen species in cellular iron metabolism. Free Radic Res. 2006; 40:263–72. [PubMed: 16484042]
32. Ziebell BT, Galan HL, Anthony RV, Regnault TR, Parker TA, Arroyo JA. Ontogeny of endothelial nitric oxide synthase mRNA in an ovine model of fetal and placental growth restriction. Am J Obstet Gynecol. 2007; 197(4):420, e1–5. [PubMed: 17904986]
33. Hentze MW, Kuhn LC. Molecular control of vertebrate iron metabolism: mRNA-based regulatory circuits operated by iron, nitric oxide, and oxidative stress. Proc Nat Acad Sci USA. 1996; 93:8175–82. [PubMed: 8710843]
34. Smith CA, Santymire B, Erdely A, Venkat V, Losonczy G, Baylis C. Renal nitric oxide production in rat pregnancy: role of constitutive nitric oxide synthases. Am J Physiol. 2010; 299(4):F830–F6.
35. Mount PF, Power DA. Nitric oxide in the kidney: functions and regulation of synthesis. Acta Physiol. 2006; 187(4):433–46.
36. Magness RR, Meyer KM, Sun MY, Ramadoss J, Kling PJ. Development of an ovine surgical model of uterine space restriction: uterine anomalies and multi-fetal gestations on placental growth and uterine vascular adaptations. J Develop Orig Health Dis. 2011; 2(Supplement 1):S95–S6.
37. Magness RR, Sullivan JA, Li Y, Phernetton TM, Bird IM. Endothelial vasodilator production by uterine and systemic arteries. VI. Ovarian and pregnancy effects on eNOS and NO(x). Am J Physiol Heart Circ Physiol. 2001; 280(4):H1692–8. [PubMed: 11247781]
38. Khong TY, Toering TJ, Erwich JJ. Haemosiderosis in the placenta does not appear to be related to chronic placental separation or adverse neonatal outcome. Pathology. 2010; 42(2):119–24. [PubMed: 20085512]
39. Saarinen UM, Siimes MA. Developmental changes in serum iron, total iron-binding capacity, and transferrin saturation in infancy. J Pediatr. 1977; 91(6):875–7. [PubMed: 925813]
40. Rebouche CJ, Wilcox CL, Widness JA. Microanalysis of non-heme iron in animal tissues. J Biochem Biophys Methods. 2004; 58:239–51. [PubMed: 15026210]
41. Schroeter M, Saleh A, Wiedermann D, Hoehn M, Jander S. Histochemical detection of ultrasmall superparamagnetic iron oxide (USPIO) contrast medium uptake in experimental brain ischemia. Magn Reson Med. 2004; 52(2):403–6. [PubMed: 15282824]
42. Shi SR, Chaiwun B, Young L, Cote RJ, Taylor CR. Antigen retrieval technique utilizing citrate buffer or urea solution for immunohistochemical demonstration of androgen receptor in formalin-fixed paraffin sections. J Histochem Cytochem. 1993; 41(11):1599–604. [PubMed: 7691930]
43. Jobe SO, Ramadoss J, Koch JM, Jiang Y, Zheng J, Magness RR. Estradiol-17beta and its cytochrome P450- and catechol-O-methyltransferase-derived metabolites stimulate proliferation in uterine artery endothelial cells: role of estrogen receptor-alpha versus estrogen receptor-beta. Hypertension. 2010; 55(4):1005–11. [PubMed: 20212268]

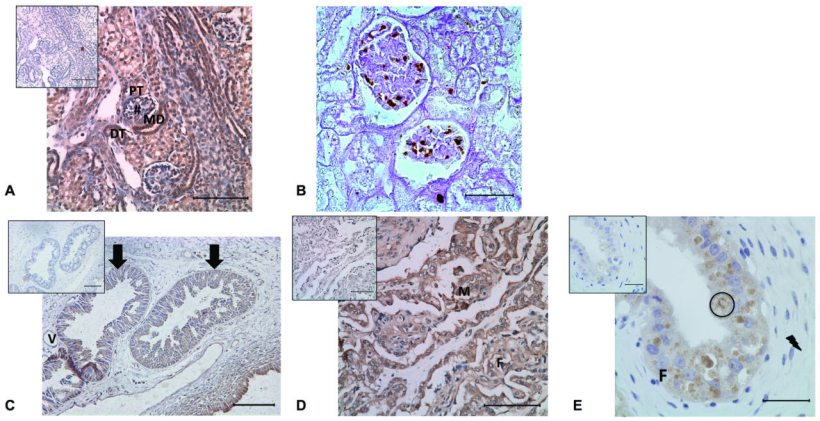

Figure 1.

Kidney and placenta histology and immunohistochemistry. A) DAB brown staining of a NSR at GD120 kidney indicating TfR localization in the distal tubule (DT), maculae densa (MD), proximal tubule (PT), and glomerulus (#) with IgG negative control on the top left corner. Sections were counterstained with hematoxylin. Bar = 100 μm. B) Enhanced PB staining in brown of iron deposits in the glomerulus of a USR at GD130 kidney. Bar = 35 μm (C) DAB brown staining of TfR seen primarily in the uterine glands of a NSR at GD130 placenta. Arrows indicate uterine glandular epithelium and interstitial tissue with (V) showing a vessel. Top left corner shows the IgG negative control. Sections were counterstained with hematoxylin. Bar = 100 μm. (D) DAB brown staining of TfR in fetal trophoblasts (F) and maternal epithelium (M) at the interdigitation of the villi and septa of a USR at GD130 placenta with the IgG negative control on the top left corner. Sections were counterstained with hematoxylin. Bar = 100 μm. (E) DAB brown staining of a NSR at GD130 placenta indicating TfR localization in the hemophagous zone with the lightning bolt showing the stroma, circle indicating ingested erythrocyte, and fetal villus (F), with IgG negative control on the top left corner. Sections were counterstained with hematoxylin. Bar = 35 μm.

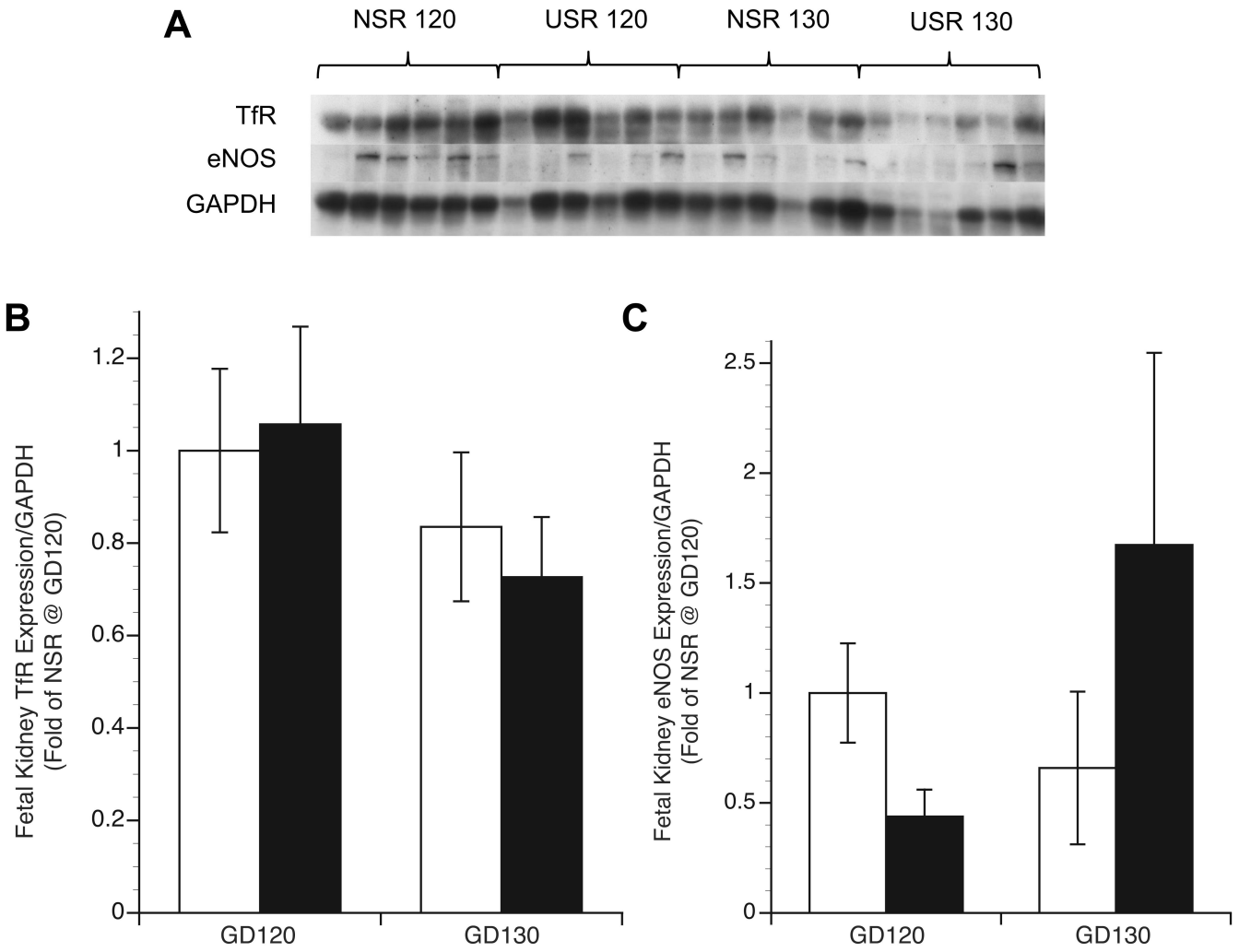

Figure 2.

Fetal kidney TfR and eNOS expression in nonrestricted (NSR) and space-restricted (USR) groups at GD120 and GD130. A) Western blot of TfR and eNOS with GAPDH as loading control in fetal kidney. B and C) Respective optical density means (fold of control NSR at GD120) and SEM. White bars: NSR, black bars: USR. *Significant difference ($P<0.05$) compared to NSR at GD120. **Significant difference ($P<0.05$) compared to USR at GD120. †Significant difference ($P<0.05$) compared to NSR at GD130.

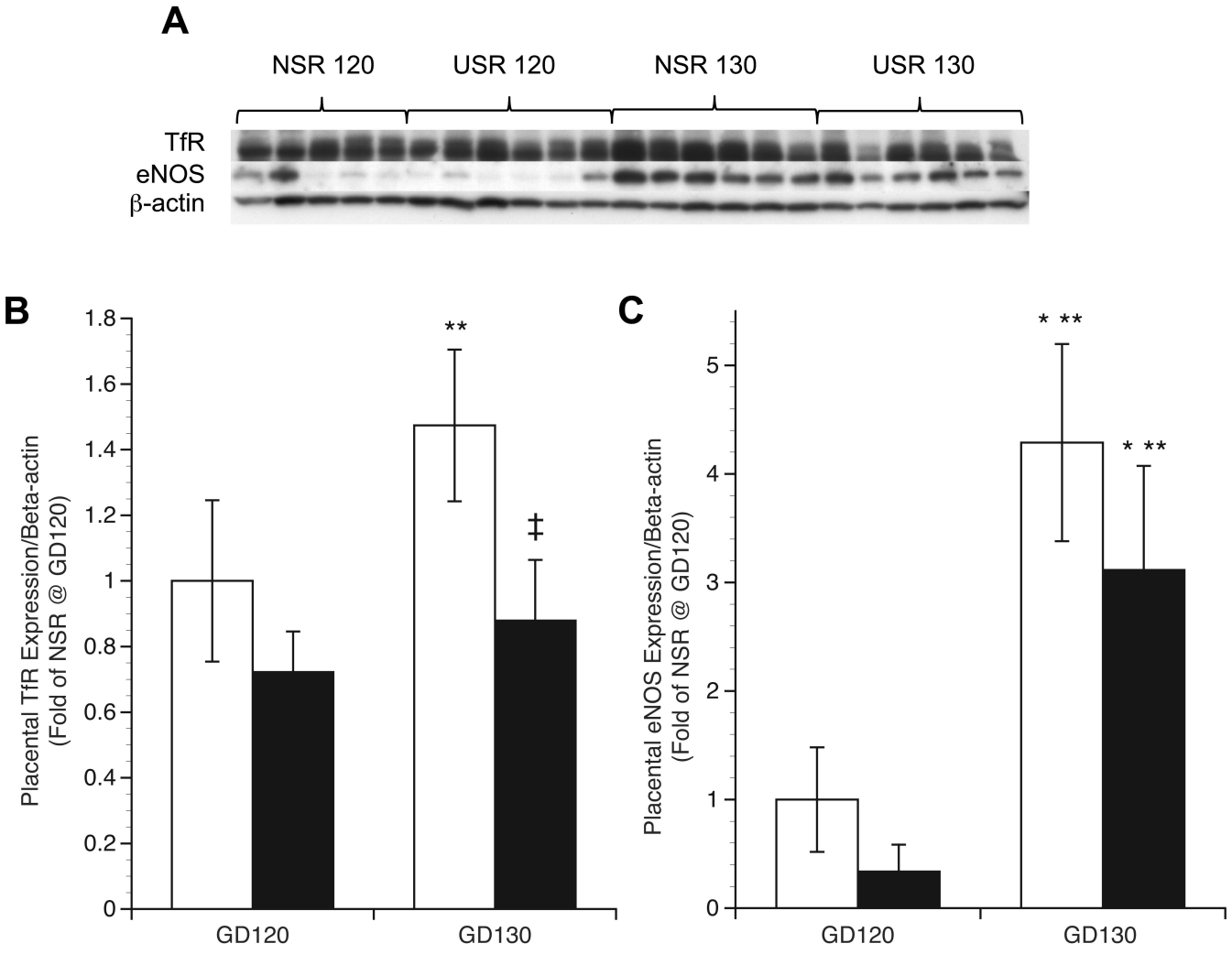

Figure 3.

Placental TfR and eNOS expression in nonrestricted (NSR) and space-restricted (USR) groups at GD120 and GD130. A) Western blot of TfR and eNOS with β-actin as loading control in the placenta. B and C) Respective optical density Means (fold of control NSR at GD120) and SEM. White bars: NSR, black bars: USR. *Significant difference (P<0.05) compared to NSR at GD120. **Significant difference (P<0.05) compared to USR at GD120. †Significant difference (P<0.05) compared to NSR at GD130.

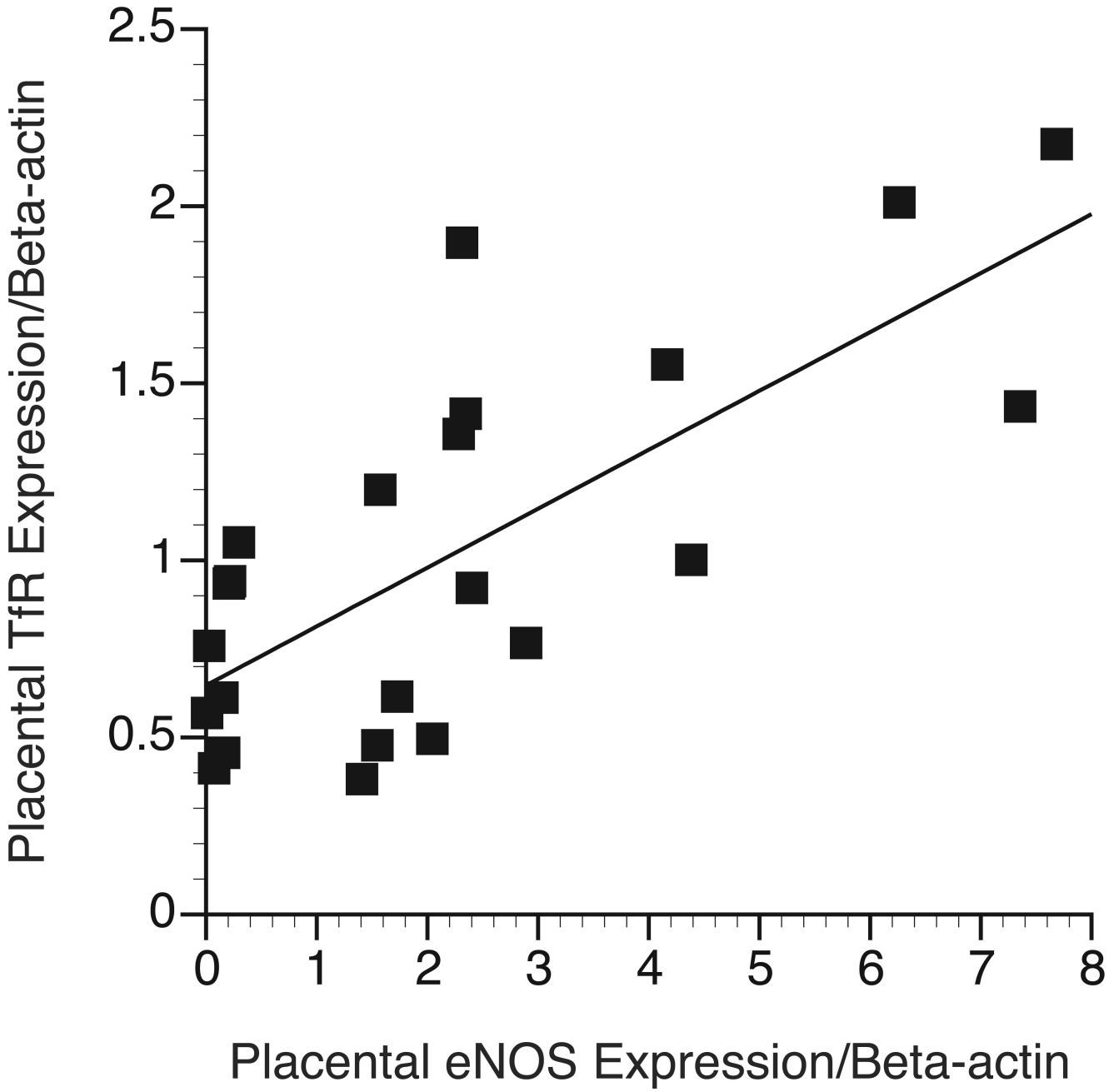

Figure 4.
Regulation of placental TfR expression. Placental eNOS expression was quantified and plotted against placental TfR expression (r=0.726; p<0.001).

Table 1

Fetal Morphometrics of Nonrestricted and Uterine Space Restricted fetuses at GD120 and GD130

	120 Days Gestation		130 Days Gestation	
	Nonrestricted (n=12)	**Restricted (n=12)**	**Nonrestricted (n=10)**	**Restricted (n=19)**
Fetal weight (kg)	2.97 ± 0.20	2.53 ± 0.19	4.27 ± 0.47*†	3.08 ± 0.17‡
Kidneys weights (g)	23.0 ± 1.1	19.5 ± 1.5	26.5 ± 2.6†	18.7 ± 0.7*†‡
Kidney weight/fetal weight (g/kg)	7.9 ± 0.3	7.8 ± 0.5	6.3 ± 0.3*†	6.2 ± 0.3*†
Liver weight (g)	107.4 ± 4.1	88.9 ± 6.0*	117.9 ± 11.5†	78.1 ± 4.2*‡
Liver weight/fetal weight (g/kg)	37.4 ± 1.7	35.7 ± 1.3	28.5 ± 1.8*†	25.8 ± 1.3*†
Placentome weight (g)	543.5 ± 24.6	1223.0 ± 36.5*	520.5 ± 52.5†	1010.0 ± 31.7*†‡
Placentome weight/fetus (g)	543.5 ± 24.6	407.5 ± 12.2*	520.5 ± 52.5†	318.8 ± 13.3*†‡

Data are Means ± SEM; n, number of fetuses. Superscripts compare nonrestricted and uterine space restricted within each gestational day (GD) and between GD.

*Significant difference ($P<0.05$) compared to Nonrestricted at 120 Days Gestation.

†Significant difference ($P<0.05$) compared to Restricted at 120 Days Gestation.

‡Significant difference ($P<0.05$) compared to Nonrestricted at 130 Days Gestation.

Table 2

Erythrocyte iron indices in maternal artery and fetal vein of Nonrestricted and Uterine Space Restricted groups at GD120 and GD130

	Maternal				Fetal			
	120 Days Gestation		130 Days Gestation		120 Days Gestation		130 Days Gestation	
	Nonrestricted (n=12)	Restricted (n=4)	Nonrestricted (n=10)	Restricted (n=6)	Nonrestricted (n=12)	Restricted (n=12)	Nonrestricted (n=10)	Restricted (n=19)
Total Fe (mg)	15.9 ± 2.1	13.2 ± 0.6	17.1 ± 1.4†	14.5 ± 0.4	17.3 ± 1.4	18.0 ± 0.8	18.1 ± 1.1	18.7 ± 0.6
RBC (mill/mm^3)	9.1 ± 0.9	7.7 ± 0.2	10.0 ± 0.7†	8.5 ± 0.2‡	8.3 ± 0.7	8.2 ± 0.4	8.5 ± 0.5	9.2 ± 0.3
Hematocrit (%)	33.8 ± 2.4	35.5 ± 1.9	31.6 ± 1.8*†	31.7 ± 0.2‡	41.7 ± 2.5	47.3 ± 4.8	38.4 ± 2.0	43.2 ± 2.4
MCV (fL)	50.5 ± 3.4	43.8 ± 0.1*	45.4 ± 0.6*	45.0 ± 0.5*	57.3 ± 1.1	59.2 ± 0.5	55.4 ± 1.2†	52.3 ± 0.9*†‡
RDW (%)	26.3 ± 1.8	25.7 ± 0.3	27.1 ± 1.0	25.4 ± 0.4	23.1 ± 0.9	24.2 ± 1.7	23.4 ± 0.4	25.0 ± 0.6
Plasma Iron (μg/dL)	145.4 ± 9.3	140.0 ± 6.8	147.8 ± 9.1	162.6 ± 10.0	210.1 ± 13.4	239.7 ± 8.5	226.6 ± 19.2	275.9 ± 11.2*†‡
[Tf] (mg/L)	354.6 ± 35.8	300.4 ± 7.2	317.0 ± 13.4	326.1 ± 4.4	274.9 ± 40.2	233.1 ± 18.0	311.4 ± 53.8	511.2 ± 33.2*†‡
Tf Saturation (%)	29.6 ± 3.0	34.8 ± 1.2*	36.0 ± 2.4*	43.9 ± 1.1*†‡	62.4 ± 7.2	71.9 ± 4.1	55.1 ± 9.0	41.2 ± 1.5*†
TIBC (μg/dL)	89.1 ± 9.0	75.5 ± 1.8	79.7 ± 3.4	82.0 ± 1.1	69.1 ± 10.1	58.6 ± 4.5	78.3 ± 13.5	128.5 ± 8.3*†‡

Data are Means ± SEM; n, number of sheep or fetuses. Maternal blood data were compared to maternal blood data. Fetal blood data were compared to fetal blood data. Superscripts compare nonrestricted and uterine space restricted within each gestation day (GD) and between GD.

*Significant difference (P<0.05) compared to Nonrestricted at 120 Days Gestation.

†Significant difference (P<0.05) compared to Restricted at 120 Days Gestation.

‡Significant difference (P<0.05) compared to Nonrestricted at 130 Days Gestation.

Table 3

Fetal Liver Nonheme Iron in Nonrestricted and Uterine Space Restricted groups at GD120 and GD130

	120 Days Gestation		130 Days Gestation	
	Nonrestricted (n=6)	**Restricted (n=6)**	**Nonrestricted (n=7)**	**Restricted (n=7)**
µg/g wet weight	7.18 ± 1.04	6.18 ± 0.95	8.36 ± 0.36†	8.36 ± 1.00
Total µg	780.0 ± 153.6	656.8 ± 110.9	1029.0 ± 158.1†	655.3 ± 136.0‡
µg/kg proportional to fetal weight	268.8 ± 43.6	222.7 ± 36.3	235.7 ± 17.3	220.7 ± 30.0

Data are Means ± SEM; n, number of fetuses. Superscripts compare nonrestricted and uterine space restricted within each gestational day (GD) and between GD.

†Significant difference ($P<0.05$) compared to Restricted at 120 Days Gestation.

‡Significant difference ($P<0.05$) compared to Nonrestricted at 130 Days Gestation.

Table 4

Fetal Kidney Nonheme Iron in Nonrestricted and Uterine Space Restricted groups at GD120 and GD130

	120 Days Gestation		130 Days Gestation	
	Nonrestricted (n=7)	**Restricted (n=6)**	**Nonrestricted (n=6)**	**Restricted (n=8)**
μg/g wet weight	0.47 ± 0.06	0.60 ± 0.06	0.40 ± 0.01†	0.63 ± 0.05‡
Total μg	10.8 ± 1.8	13.7 ± 1.2*	10.0 ± 0.7†	12.3 ± 1.4
μg/kg proportional to fetal weight	3.8 ± 0.4	5.2 ± 0.7*	2.4 ± 0.2*†	3.8 ± 0.3†‡

Data are Means ± SEM; n, number of fetuses. Superscripts compare nonrestricted and restricted within each gestational day (GD) and between GD.

*Significant difference ($P<0.05$) compared to Nonrestricted at 120 Days Gestation.

†Significant difference ($P<0.05$) compared to Restricted at 120 Days Gestation.

‡Significant difference ($P<0.05$) compared to Nonrestricted at 130 Days Gestation.

Table 5

Number of Ewes and Fetuses within Treatment Groups

	Treatment	Ewes (n=32)	Fetuses (n=53)
NSR	Non-unilateral	9	9 (all singleton)
	Unilateral	13	13 (all singleton)
USR	Non-unilateral	8	25 (2 triplets)
	Unilateral	2	6 (7 triplets, 1 quad)